Journal of Physics: Conference Series

PAPER • **OPEN ACCESS**

Human chest imaging by real-time processing of electrical impedance data tomography

To cite this article: G Gottardi and L Poli 2018 *J. Phys.: Conf. Ser.* **1131** 012003

View the article online for updates and enhancements.

IOP ebooks™

Bringing you innovative digital publishing with leading voices to create your essential collection of books in STEM research.

Start exploring the collection - download the first chapter of every title for free.

This content was downloaded from IP address 151.49.207.248 on 02/01/2019 at 11:06

IOP Conf. Series: Journal of Physics: Conf. Series **1131** (2018) 012003 doi:10.1088/1742-6596/1131/1/012003

Human chest imaging by real-time processing of electrical impedance data tomography

G Gottardi[1] **and L Poli**[1]

[1] ELEDIA Research Center (ELEDIA@UniTN - University of Trento)
Via Sommarive 9, I-38123 Trento, Italy

E-mail: lorenzo.poli@unitn.it

Abstract. Real-time human chest imaging exploiting electrical impedance tomography (*EIT*) data is addressed in this work. Robust estimations of the lungs conductivity, directly related to their air/liquid content, are obtained by formulating the arising inverse problem within the learning-by-examples (*LBE*) framework. The partial least squares (*PLS*) algorithm is exploited to reduce the dimensionality of the feature space, while an adaptive sampling strategy is exploited to build an optimal training set of input/output pairs used to build a computationally efficient surrogate model of the inverse operator. Selected numerical results are shown to assess the effectiveness and the potentialities of the proposed *LBE* strategy.

1. Introduction

Electrical impedance tomography (*EIT*) is a promising alternative to computed tomography (*CT*) and X-ray radiography in many medical non-invasive diagnosis applications including breast cancer detection and heart/brain/lungs activity monitoring [1]-[6]. Differently from both standard investigation technologies, *EIT* provides lower resolution images of the investigated domain but it doesn't expose the patient to ionizing radiation. Moreover, it allows a continuous low-cost and easy-deployable monitoring, which is fundamental in some clinical scenarios such as, for example, the monitoring of the air content of the lungs in patients under mechanical ventilation in intensive-care units. Within this applicative context, low-frequency currents are induced in the chest through pairs of electrodes attached to the patient skin. The conductivity distribution within the inspected domain (strongly related to the air/liquid content of the lungs) determines the resulting voltages measured at other pairs of electrodes, allowing to retrieve - through suitable processing - a cross-sectional image of the human thorax [1]-[6].

The poor signal-to-noise ratio as well as the limited number of independent measurements lead to a severely *non-linear* and *ill-posed* inverse problem, for which suitable reconstruction algorithms and regularization schemes have to be carefully developed and/or customized. As an example, Tikhonov-based [5] or sparseness-based [6]-[10] regularizations can be successfully exploited to address the solution of the inverse *EIT* problem. Alternatively, learning-by-examples (*LBE*) methods can be regarded as computationally-efficient approaches to achieve real-time guesses of the imaged domain without exploiting iterative (costly) evaluations of the forward operator [11]-[19].

LBE strategies are based on a two-step procedure aimed at (*a*) generating a suitable set of input/output (*I/O*) examples in order to train a surrogate model during the *off-line phase* and (*b*) exploiting such a trained model to make fast and accurate predictions during the *on-line phase* starting

Content from this work may be used under the terms of the Creative Commons Attribution 3.0 licence. Any further distribution of this work must maintain attribution to the author(s) and the title of the work, journal citation and DOI.
Published under licence by IOP Publishing Ltd

from previously-unseen data [11]. Within this context, this work presents a novel *LBE* strategy for the real-time estimation the conductivity of the human lungs from *EIT* measurements. The developed inversion technique exploits the innovative integration of the partial least squares (*PLS*) feature extraction technique with an adaptive sampling scheme aimed at generating an optimal (i.e., highly-informative and reduced-size) training set [13], which is in turn used to train an augmented radial basis function (*A-RBF*) predictor [20].

2. Mathematical formulation

Let us consider a two-dimensional bounded investigation domain D representing a cross-section of the human thorax (Fig. 1). The conductivity distribution within D, $\sigma(x,y)$, is assumed to be purely real (resistive) and piecewise constant depending on the organ/tissue (i.e., lungs, muscle, fat, and hearth - Fig. 1).

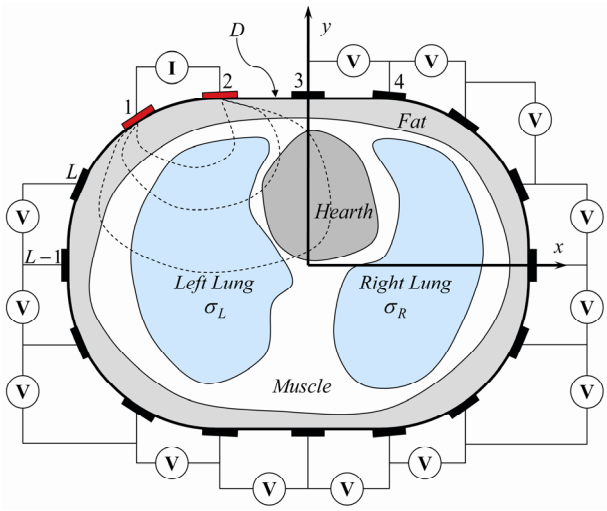

Figure 1. Geometry of the *2D* human thorax model and *EIT* acquisition system.

The adjacent electrode pair measurement strategy [2] is considered to collect *EIT* data exploiting a set of L electrodes uniformly displaced over the external boundary of D (Fig. 1). Accordingly, a low-frequency current (i.e., $f < 100\,\text{kHz}$) is successively applied to each pair of electrodes, the resulting voltages being measured over all remaining $(L-3)$ adjacent pairs of electrodes (Fig. 1). The total number of independent measurements is thus equal to [1]

$$M = \frac{L(L-3)}{2} \tag{1}$$

A standard finite element method (*FEM*) is used to numerically treat the forward problem, by sub-dividing D into N triangular mesh cells [2]. Accordingly, the set of measured voltages corresponding to a given conductivity distribution within D, $\boldsymbol{\sigma} = \{\sigma(x_n, y_n); n = 1,...,N\}$, is computed exploiting the low-frequency approximation through the Poisson equation [2], resulting in

$$\mathbf{V} = \Phi\{\boldsymbol{\sigma}\} \tag{2}$$

where $\mathbf{V} = \{V_m; m = 1,...,M\}$ and $\Phi\{.\}$ represents the forward *2D EIT-FEM* operator.

The goal of the inverse problem is to estimate the conductivity value inside the regions occupied by the left ($\sigma(x,y) = \sigma_L$) and right ($\sigma(x,y) = \sigma_R$) lungs, which is directly proportional to the their air/liquid content, by assuming that the conductivity of the neighboring regions (i.e., fat, muscle, and heart - Fig. 1) is fixed and a-priori known. In other words, a suitable inversion scheme must be

adopted in order to estimate the unknown vector $\mathbf{\Omega}=(\sigma_L,\sigma_R)$ starting from the corresponding set of *EIT* voltages, i.e., solving the following implicit-form expression

$$\widetilde{\mathbf{\Omega}}=\widetilde{\Phi}^{-1}\{\mathbf{V}\} \tag{3}$$

where the hat "~" indicates that inverse operator $\Phi^{-1}\{.\}$ can be only approximated since it is unknown. To solve the inverse problem (3) an innovative inversion strategy is proposed in the framework of the learning-by-examples (*LBE*) theory [11]. Thanks to such a technique, the information about the two lungs embedded inside *EIT* measurements can be effectively *compressed* into a very small-dimensional features space, which is in turn adaptively sampled by an iterative sampling scheme in order to accurately model the *I/O* relationship with a limited set of training samples/observations. The solution of (3) is obtained through the following procedural steps.

1. *Initialization*. In order to adaptively sampling the two-dimensional space identified by $\mathbf{\Omega}$, the first step is to generate an initial set of *I/O* pairs. Towards this end, the Latin hypercube sampling (*LHS*) strategy is applied to randomly sample the input space and generate $S=S_0$ configurations (within predefined variation ranges)

$$\mathbf{\Omega}^s=\left(\sigma_L^s,\sigma_R^s\right),\ s=1,...,S_0\,. \tag{4}$$

For each input sample, the forward *EIT-FEM* problem is solved in order to compute the corresponding *EIT* data, i.e.,

$$\mathbf{V}^s=\left(V_m^s;m=1,...,M\right)=\Phi\left\{\mathbf{\Omega}^s\right\},\ s=1,...,S_0\,. \tag{5}$$

Both input samples and corresponding outputs are then used to fill two matrices, i.e.,

$$\boldsymbol{\sigma}_0=\begin{bmatrix}\sigma_L^1 & \sigma_R^1\\ \sigma_L^2 & \sigma_R^2\\ \vdots & \vdots\\ \sigma_L^{S_0} & \sigma_R^{S_0}\end{bmatrix};\quad \mathbf{V}_0=\begin{bmatrix}V_1^1 & V_2^1 & \dots & V_M^1\\ V_1^2 & \ddots & & \vdots\\ \vdots & & & \vdots\\ V_1^{S_0} & V_2^{S_0} & \dots & V_M^{S_0}\end{bmatrix}. \tag{6}$$

2. *Feature Extraction*. Instead of directly exploiting the *M*-dimensional measured voltages for solving the inverse problem, the information about $\boldsymbol{\sigma}_0$ embedded within $\mathbf{V}_0$ is *compressed* into a small set of $J<<M$ features through the partial least squares (*PLS*) algorithm. Thanks to such an approach, it is possible to (*i*) mitigate the *curse of dimensionality* [11] when solving the inverse problem, since a lower number of training samples will be necessary for an accurate modeling of $\Phi^{-1}\{.\}$, and (*ii*) filter a large amount of noise normally affecting *EIT* measurements. Accordingly, the SIMPLS algorithm [13] is exploited to compute from $\boldsymbol{\sigma}_0$ and $\mathbf{V}_0$ the *PLS* weight matrix $\mathbf{W}$ allowing to compute the *extracted features matrix*

$$\mathbf{T}_0=\begin{bmatrix}T_1^1 & T_2^1 & \dots & T_J^1\\ T_1^2 & \ddots & & \vdots\\ \vdots & & & \vdots\\ T_1^{S_0} & T_2^{S_0} & \dots & T_J^{S_0}\end{bmatrix} \tag{7}$$

through a linear combination of the original *measured features*, i.e.,

$$\mathbf{T}_0=\mathbf{V}_0\mathbf{W}\,. \tag{8}$$

Each row of $\mathbf{T}_0$ contains the J extracted features associated to a given input (σ_L,σ_R) configuration, and can be used in substitution to the corresponding (*M*-dimensional) row of $\mathbf{V}_0$. The initial training set is then formed with the generated S_0 *I/O* pairs as follows

$$\mathbf{\Psi}_0=\left\{\left(\left(T_j^s;j=1,...,J\right),\left(\sigma_L^s,\sigma_R^s\right)\right),s=1,...,S_0\right\} \tag{9}$$

3. *Adaptive Sampling*. Once the *PLS* matrix **W** has been determined, it is possible to map additional *EIT* measurements into the *J*-dimensional space of extracted features. The generation of new training samples is done by adaptively sampling the $\mathbf{\Omega}$ space, such that a uniform coverage of the extracted features space is obtained [13]. At each iteration of such an adaptive scheme, a set of C candidates, $\left(\sigma_L^c,\sigma_R^c\right)$, $c=1,...,C$, is generated via *LHS* sampling. The goal is to select the candidate $\mathbf{\Omega}^*$ that exhibits the largest minimum Euclidean distance in the extracted features space to all previously collected *S* training samples (being $S=S_0$ at the first iteration), i.e.,

$$\mathbf{\Omega}^*=\left(\sigma_L^*,\sigma_R^*\right)=\arg\left(\max_{c=1,...,C}\left\{\min_{s=1,...,S}\sqrt{\sum_{j=1}^{J}\left(T_j^c-T_j^s\right)^2}\right\}\right). \tag{10}$$

In order to avoid the evaluation of the extracted features associated to each candidate, which would require the repeated solution of the forward *EIT-FEM* problem (with a significant waste of computational resources), a fast linear interpolator is exploited on the existing training samples to predict T_j^c, $j=1,....,J$, $c=1,...,C$ [13]. Then, once $\mathbf{\Omega}^*$ has been identified through (10), the actual *PLS* features associated to such sample are determined by computing (now only once) the associated *EIT* voltages, i.e., $\mathbf{V}^*=\left(V_m^*;m=1,...,M\right)=\Phi\left\{\sigma_L^*,\sigma_R^*\right\}$, and transforming them through the matrix **W** (i.e., $\mathbf{T}^*=\left(T_j^*;j=1,...,J\right)=\mathbf{V}^*\mathbf{W}$). The training set is then updated by adding the selected *I/O* pair

$$\mathbf{\Psi}_S=\mathbf{\Psi}_{S-1}\cup\left\{\mathbf{T}^*;\mathbf{\Omega}^*\right\} \tag{11}$$

and the process is iterated until a predefined stopping criterion is met (e.g., when a maximum number of forward solver evaluations, $S_{\max}$, is reached).

4. *Prediction*. Once the training set has been adaptively generated, it can be used to build a prediction model which will be able to estimate the lungs conductivities starting from previously-unseen *EIT* measurements. In this work, the augmented radial basis function (*A-RBF*) technique [20] is used to build such a model given its numerical efficiency and the need to calibrate only a single parameter, i.e., the width of the *RBF* kernel function, γ. During the on-line test phase, each new test *EIT* measurement is first converted through **W** to the corresponding set of *J* extracted features, and then given as input to the trained *A-RBF* model to estimate the corresponding lungs conductivities.

3. Numerical validation

In order to verify the effectiveness of the proposed *LBE* inversion strategy for real-time *EIT* lungs monitoring, a set of numerical experiments is carried out considering $L=16$ electrodes surrounding *D*, resulting into $M=104$ independent voltage measurements. The human thorax is sub-divided into $N=3130$ triangular mesh cells, while the conductivity of the heart, fat, and muscle are set according to the low−frequency tissue properties table of the IT'IS Foundation [21] to 3.81×10^{-1} S/m, 5.73×10^{-2} S/m, and 3.55×10^{-1} S/m, respectively (Fig. 1). To build the training set, the left and right lungs conductivities are varied within the range $\left(\sigma_L,\sigma_R\right)\in\left[4.18\times10^{-2},8.05\times10^{-1}\right]$S/m. The initial training set consists of $S_0=25$ *LHS*-generated samples, while $J=2$ is the number of *PLS*-extracted features (carefully set after a preliminary calibration process). To test the robustness of the inversions against noise, an additive white Gaussian noise is considered to corrupt *EIT* measurements with different signal-to-noise-ratios (*SNR*s).

To provide a pictorial view of the achievable estimation accuracy, Figure 2 shows the scatter plot of the actual versus predicted conductivity for the left [Figs. 2(*a*),2(*c*)] and right [Figs. 2(*b*),2(*d*)] lungs when training the *A-RBF* with $S=S_{\max}=225$ training samples and testing it over $K=1000$ *LHS*-

generated noisy *EIT* test measurements at $SNR = 40$ dB [Figs. 2(*a*)-2(*b*)] and $SNR = 20$ dB [Figs. 2(*c*)-2(*d*)].

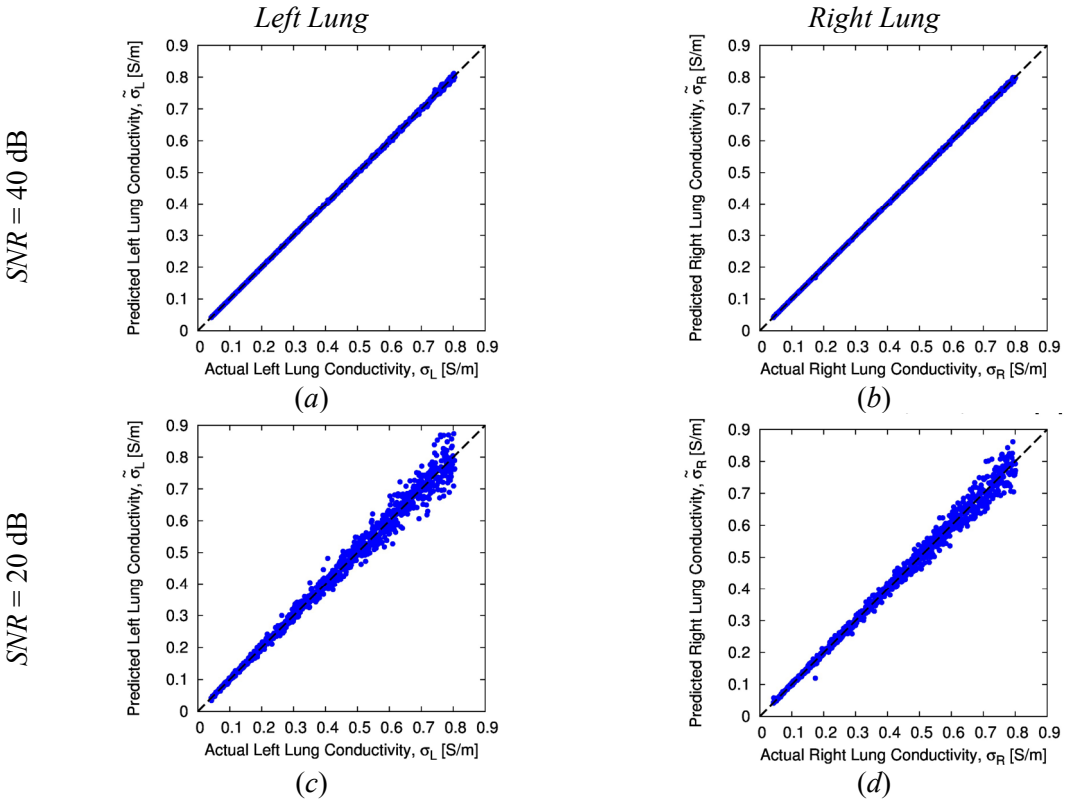

Figure 2. *Numerical Assessment* ($M = 104$, $J = 2$, $S = 225$) - Actual vs. predicted (*a*)(*c*) left and (*b*)(*d*) right lung conductivity when processing noisy data at (*a*)(*b*) $SNR = 40$ dB and (*c*)(*d*) $SNR = 20$ dB.

As it can be observed, a very high prediction accuracy is yielded at both levels of noise, with accurate guesses of the left and right conductivities within the considered variation ranges.

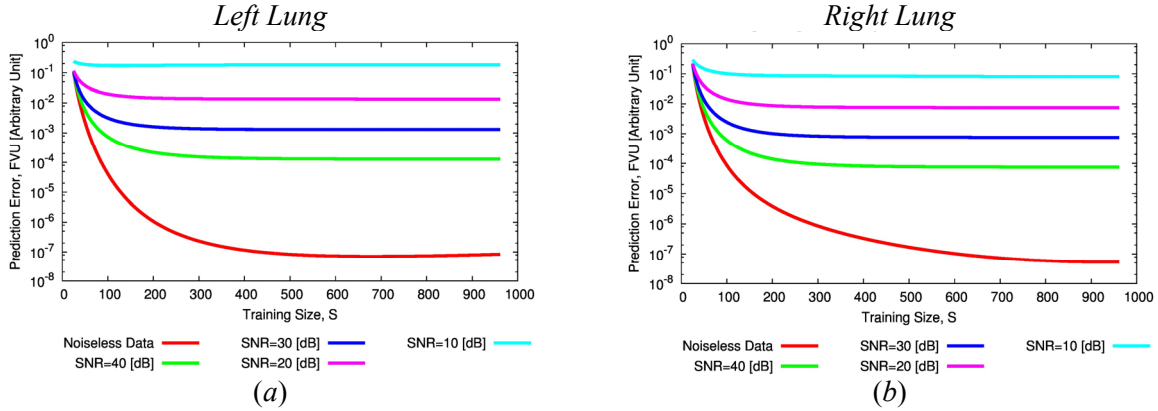

Figure 3. *Numerical Assessment* ($M = 104$, $J = 2$, $S = 225$) - Behaviour of the prediction error versus the number of training samples for (*a*) left and (*b*) left lung conductivity estimation.

To have a wider overview of the achievable prediction performances, Figure 3 shows the behaviour of the prediction error versus the number of training samples, *S*, used to train the *A-RBF*. The reported error is defined as the fraction of unexplained variance (*FVU*), computed as follows

$$FVU = \frac{\sum_{k=1}^{K}(\sigma_k - \tilde{\sigma}_k)^2}{\sum_{k=1}^{K}(\sigma_k - \sigma_{av})^2} \tag{12}$$

where σ_k and $\tilde{\sigma}_k$ are the actual and predicted conductivity for the *k*-th test sample, and $\sigma_{av} = \frac{1}{K}\sum_{k=1}^{K}\sigma_k$ is the average conductivity within the test samples. It is worth observing that the error rapidly drops as new training samples are adaptively added to the initial ones (Fig. 3). Moreover, the error turns out to be always $FVU < 1$ whatever the *SNR* and the training size, meaning that the *A-RBF* is capable of providing better estimations with respect to the most naive predictor (which would output for each test sample the average conductivity value, thus yielding $FVU = 1$). As for what concerns the required computational times for the inversion, the *PLS* algorithm extracts the *J* features from a new measurement within fraction of seconds ($\Delta t^{PLS} \approx 10^{-2}$ sec), while the *A-RBF* is able to output a prediction of the lungs conductivities in about $\Delta t^{A-RBF} \approx 10^{-1}$ sec. Accordingly, it is possible to confirm that the whole inversion process is almost performed in real-time as soon as new *EIT* data is available from the acquisition system.

4. Conclusions

The computationally-efficient inversion of *EIT* data for monitoring the air content in human lungs has been addressed through an innovative *LBE* inversion strategy. Thanks to the *PLS* feature extraction a significant compression of the informative features can be obtained, allowing both a reduction of the necessary training samples to accurately model the *I/O* relation and an effective noise filtering during the on-line test phase. It should be remarked that the proposed methodology is not aimed at retrieving a full image of the conductivity distribution within the chest (as done in classical imaging), but rather at estimating the value of some monitored parameters of clinical relevance. Of course, these latter are not necessarily limited to the lungs conductivities, since the proposed approach is very flexible and customizable to the needs of the specific application. Selected numerical results have been presented to assess the effectiveness of the proposed strategy, as well as to confirm its capability of performing almost instantaneous inversions. Future works will be devoted at extending the capabilities of the *LBE* method to estimate other parameters of interest within the human thorax form *EIT* data, as well as to consider a fully-*3D* modeling of the forward problem. Moreover, further studies will be devoted at studying the robustness of the linearity assumption made by the *PLS* algorithm, as well as to validate the approach against real *EIT* data.

Acknowledgment

This work has been partially supported by the Italian Ministry of Foreign Affairs and International Cooperation, Directorate General for Cultural and Economic Promotion and Innovation within the SNATCH Project (2017-2019).

References

[1] Brown BH 2003 Electrical impedance tomography (EIT): a review *J. Med. Eng. Technol.* **27** 97-108

[2] Denaï MA, Mahfouf M, Mohamad-Samuri S, Panoutsos G, Brown BH and Mills GH 2010 Absolute electrical impedance tomography (aEIT) guided ventilation therapy in critical care

patients: simulations and future trends *IEEE Trans. Inf. Technol. Biomed.* **14** 641-649
[3] Borcea L 2002 Electrical impedance tomography *Inverse Probl.* **18** R99-R136
[4] Moura FS, Aya JCC, Fleury AT, Amato MBP and Lima RG 2010 Dynamic imaging in electrical impedance tomography of the human chest with online transition matrix identification *IEEE Trans. Biomed. Eng.* **57** 422-431
[5] Vauhkonen M, Vadasz D, Karjalainen PA, Somersalo E and Kaipio JP 1998 Tikhonov regularization and prior information in electrical impedance tomography *IEEE Trans. Med. Imag.* **17** 285-293
[6] Gehre M, Kluth T, Lipponen A, Jin B, Seppänen A, Kaipio J and Maass P 2012 Sparsity reconstruction in electrical impedance tomography: an experimental evaluation *J. Comput. Appl. Math.* **236** 2126-2136
[7] Oliveri G, Salucci M, Anselmi N and Massa A 2017 Compressive sensing as applied to inverse problems for imaging: theory, applications, current trends, and open challenges *IEEE Antennas Propag. Mag*. **59** 34-46
[8] Anselmi N, Oliveri G, Hannan M A, Salucci M and Massa A 2017 Color compressive sensing imaging of arbitrary-shaped scatterers *IEEE Trans. Microw. Theory Techn.* **65** 1986-1999
[9] Anselmi N, Oliveri G, Salucci M and Massa A 2015 Wavelet-based compressive imaging of sparse targets *IEEE Trans. Antennas Propag.* **63** 4889-4900
[10] Salucci M, Gelmini A, Poli L, Oliveri G and Massa A 2018 Progressive compressive sensing for exploiting frequency-diversity in GPR imaging *Journal of Electromagnetic Waves and Applications,* in press
[11] Massa A, Oliveri G, Salucci M, Anselmi N and Rocca P 2018 Learning-by-examples techniques as applied to electromagnetics *J. Electromagn. Waves Appl.* **32** 516-541
[12] Demidenko E, Hartov A and Paulsen K 2004 Statistical estimation of resistance/conductance by electrical impedance tomography measurements *IEEE Trans. Med. Imag.* **23** 829-838
[13] Salucci M, Anselmi N, Oliveri G, Calmon P, Miorelli R, Reboud C and Massa A 2016 Real-time NDT-NDE through an innovative adaptive partial least squares SVR inversion approach *IEEE Trans. Geosci. Remote Sens.* **54** 6818-6832
[14] Salucci M, Vrba J, Merunka I and Massa A 2017 Real-time brain stroke detection through a learning-by-examples technique - an experimental assessment *Microw. Opt. Technol. Lett.* **59** 2796-2799
[15] Li M, Abubakar A and Habashy TM 2012 A three-dimensional model-based inversion algorithm using radial basis functions for microwave data *IEEE Trans. Antennas Propag.* **60** 3361-3372
[16] Wu Y, Tang ZX, Zhang B and Xu Y 2007 Permeability measurement of ferromagnetic materials in microwave frequency range using support vector machine regression *Prog. Electromagn. Res.* **70** 247-256
[17] Ahmed S, Salucci M, Miorelli R, Anselmi N, Oliveri G, Calmon P, Reboud C and Massa A 2017 Real time groove characterization combining partial least squares and SVR strategies: application to eddy current testing *J. Phys. Conf. Ser.* **904** 1-8
[18] Ahmed S, Miorelli R, Salucci M and Massa A 2017 Real-time flaw characterization through learning-by-examples techniques: a comparative study applied to ECT *Electromagnetic Nondestructive Evaluation (XX)* **42** 228-235
[19] Viani F, Migliore MD, Polo A, Salucci M and Massa A 2018 Iterative classification strategy for multi-resolution wireless sensing of passive targets *Electron. Lett.* **54** 101-103
[20] Sui YK, Li SP and Guo YQ 2008 An efficient global optimization algorithm based on augmented radial basis function *Int. J. Simul. Multisci. Des. Optim.* **2** 49-55
[21] IT'IS Foundation, Low Frequency (Conductivity) Tissue Properties, https://www.itis.ethz.ch/virtual−population/tissue−properties/database/low−frequency−conductivity